

Inversion of the exciton built-in dipole moment in In(Ga)As quantum dots via nonlinear piezoelectric effect

Johannes Aberl,^{1,*} Petr Klenovský,^{2,3,†} Johannes S. Wildmann,¹ Javier Martín-Sánchez,¹ Thomas Fromherz,¹ Eugenio Zallo,^{4,5} Josef Humlíček,^{2,3} Armando Rastelli,¹ and Rinaldo Trotta^{1,‡}

¹*Institute of Semiconductor and Solid State Physics,*

Johannes Kepler University Linz, Altenbergerstraße 69, A-4040 Linz, Austria

²*Department of Condensed Matter Physics, Masaryk University, Kotlářská, CZ-61137 Brno, Czech Republic*

³*Central European Institute of Technology, Masaryk University,*

Kamenice 753/5, CZ-62500 Brno, Czech Republic

⁴*Institute for Integrative Nanosciences, IFW Dresden, Helmholtzstraße 20, D-01069 Dresden, Germany*

⁵*Paul-Drude-Institut für Festkörperelektronik, Hausvogteiplatz 5-7, 10117 Berlin, Germany*

(Dated: July 3, 2021)

We show that anisotropic biaxial stress can be used to tune the built-in dipole moment of excitons confined in In(Ga)As quantum dots up to complete erasure of its magnitude and inversion of its sign. We demonstrate that this phenomenon is due to piezoelectricity. We present a model to calculate the applied stress, taking advantage of the so-called piezotronic effect, which produces significant changes in the current-voltage characteristics of the strained diode-membranes containing the quantum dots. Finally, self-consistent $\mathbf{k} \cdot \mathbf{p}$ calculations reveal that the experimental findings can be only accounted for by the nonlinear piezoelectric effect, whose importance in quantum dot physics has been theoretically recognized although it has proven difficult to single out experimentally.

PACS numbers: 78.67.Hc, 73.21.La, 85.35.Be, 77.65.Ly

I. INTRODUCTION

Semiconductor quantum dots (QDs) are currently emerging as one of the most promising sources of nonclassical light on which to base future quantum technologies¹. This success is in large part due to the outstanding experimental and theoretical work on QD physics that has been carried out over the last decades. These studies have not only enabled a detailed understanding of the fundamental properties of these “artificial atoms”, but have also offered the means to tailor their interactions with the environment, which is the key to make them suitable for envisioned applications.

In spite of these accomplishments, however, the extreme sensitivity of the electronic properties of QDs to tiny variations of their shape, size, composition, built-in strain fields, as well as to external perturbations² very often makes it difficult to single out the physical effects which are responsible for particular experimental observations. This is especially true for statistical studies performed on dissimilar QDs that aim at grasping general trends applicable to all of them. To explain this point further, we focus on the effect of piezoelectric fields, whose importance in theoretical semiconductor physics is well documented^{3–6}. Seminal works have demonstrated that in conventional III-V QDs grown on (100) substrates, first- and second-order contributions to the piezoelectric field tend to oppose each other so that its total effect on the QD properties is found to be small^{7,8}. This is clearly not the case for GaN QDs^{9,10} and CdSe nanocrystals¹¹, but for In(Ga)As QDs, which are usually grown on non-polar GaAs(001) substrates and are of interest for quantum optics, piezoelectricity is very often neglected^{12,13}. From the experimental side it is not straightforward to

recognize its importance. Despite the weak effect on the energy of the states, piezoelectricity is expected to have a strong influence on the position and shape of the electron and hole wave functions⁷ and, in turn, on the sign and magnitude of the exciton (X) built-in dipole moment. Early experiments¹⁴ showed that the sign of the built-in dipole moment is inverted with respect to the predicted sign¹⁵, a fact which was mainly explained by the shape and composition of the investigated QDs. In contrast, subsequent studies performed with In(Ga)As QDs grown on high-index substrates with polar orientation¹⁶ demonstrated that the observed electron-hole alignment is not a general feature, and that piezoelectricity has to be taken into account for a correct interpretation of the experimental results, as confirmed very recently¹⁷. Related experiments have demonstrated that the sign of the X dipole can even vary for different QDs within the same sample¹⁸. It is therefore rather evident that it is experimentally challenging to single out the role of piezoelectricity in QDs.

In this paper, we demonstrate that externally induced anisotropic strain fields can be used for wave function engineering and to even force an inversion of the exciton built-in dipole moment in the very same In(Ga)As QD. We achieve this result by integrating light-emitting-diode (LED) nanomembranes onto a piezoelectric actuator [see Fig. 1(a)] capable of delivering variable strain fields^{19,20}. Differently from previous results²¹ revealing a strain-dependence of the X dipole moment, we demonstrate that its tuning (and inversion) is driven by the piezoelectric effect. The induced piezoelectric field was estimated by exploiting a piezotronic-like phenomenon in the LED used²², i.e., a sizable strain-induced shift of its current-voltage (I - V) characteristics. Finally, self-

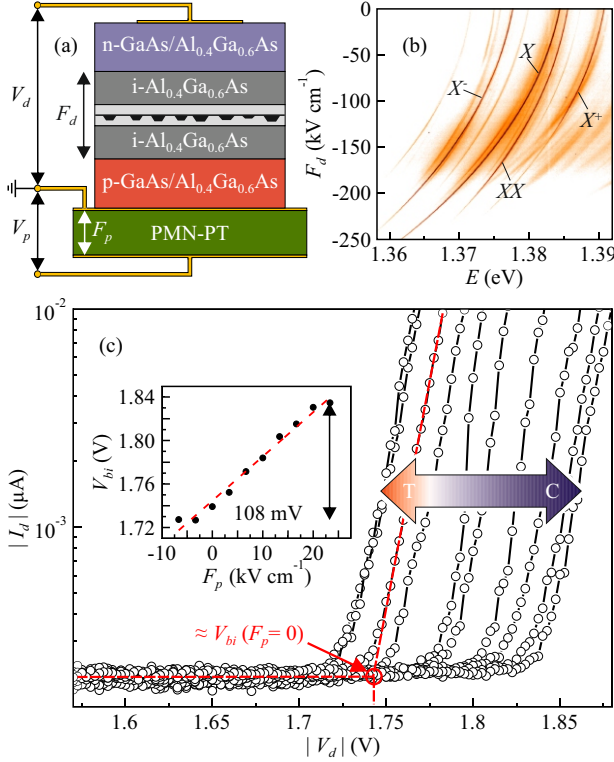


FIG. 1. (a) Sketch of the p-i-n diode bonded onto a PMN-PT piezoelectric substrate. The investigated In(Ga)As QDs were embedded in the central i-GaAs layer (light grey). The emission properties of the QDs can be tuned by using voltages applied to PMN-PT (V_p) and diode (V_d). The color-coded μ -PL map in panel (b) shows the transition energies of exciton (X), biexciton (XX), negative and positive trions (X^- , X^+) of a single QD as a function of the electric field across the diode F_d (for $F_p = 0$). (c) Shift of the I - V traces (I_d and V_d are negative in the displayed range) of the diode in response to applied stress (tensile, T or compressive, C). The built-in voltage V_{bi} was estimated from the intersection of the fitted part of the forward bias region with the saturation current (red line). The shift of V_{bi} for different steps of F_p is ascribed to the piezotronic effect and is provided in the inset.

consistent $\mathbf{k} \cdot \mathbf{p}$ calculations reveal that the inversion of the dipole moment is dominated by the nonlinear terms of the piezoelectric field.

II. EXPERIMENTAL METHODS

The microphotoluminescence (μ -PL) measurements were performed at low temperatures (8K) by using a helium flow cryostat. A femtosecond Ti-sapphire-laser (operated at 850nm) was focused by a microscope objective (0.42 numerical aperture) to address single QDs. The μ -PL spectra were recorded via a spectrometer connected to a liquid-nitrogen-cooled charge-coupled device. Polarization-resolved measurements were performed using a combination of a rotatable $\lambda/2$ wave plate and a

fixed linear polarizer placed in front of the spectrometer in order to identify the origin of the transitions in the μ -PL spectra [see Fig. 1(b)] and to estimate the exciton fine-structure splitting (FSS). The p-i-n diode nanomembrane containing In(Ga)As QDs was grown by molecular beam epitaxy. The nanomembrane was transferred via a flip-chip process and bonded onto a $[\text{Pb}[\text{Mg}_{1/3}\text{Nb}_{2/3}]\text{O}_3]_{0.72}-[\text{PbTiO}_3]_{0.28}$ (PMN-PT) piezoelectric actuator by gold thermo-compression bonding (for further details on the sample structure and device fabrication see Refs. 19 and 20). The emission properties of the QDs can be varied using two “tuning knobs”: stress and electric fields, which are applied via voltages V_p and V_d , respectively. A positive (negative) voltage V_p applied to the PMN-PT induces a compressive (tensile) anisotropic biaxial stress in the nanomembrane. The corresponding electric field across the PMN-PT is given by $F_p = V_p/d_p$, where $d_p \approx 300\mu\text{m}$ is its thickness. The electric field across the LED is instead given by $F_d = -(V_d + V_{bi})/d_d$, where $-1.9\text{V} < V_d < 1.9\text{V}$ is the applied voltage, V_{bi} the diode’s built-in voltage (positive) and $d_d \approx 150\text{nm}$ the thickness of the intrinsic region. For operation in reverse bias, F_d is oriented parallel to the QD’s growth direction, i.e. from top to bottom in Fig. 1(a). Increasing the magnitude of F_d leads to a red-shift of all transitions, as shown in Fig. 1(b).

III. TUNING OF THE X ELECTRIC DIPOLE MOMENT

We now show how strain can be used to invert the X built-in dipole moment. We start out by fitting the measured Stark shift of the X transition via

$$E = E_0 - pF_d + \beta F_d^2 \quad (1)$$

where E_0 is the transition energy at $F_d = 0$, $p = ez$ the built-in dipole moment (e elementary charge, z is the carrier separation along the growth direction), and β the polarizability²³. Repeating this procedure for each value of F_p allows us to extract the stress dependence of E_0 , p and β , as illustrated in Fig. 2(a). Obviously, the determination of these parameters is tightly connected to the use of correct values of F_d and therefore of V_{bi} , which can be estimated from the I - V trace of the diode [see Fig. 1(c)]. Herein it turned out that there is a substantial shift of V_{bi} with applied stress of up to $\Delta V_{bi} = 108\text{mV}$ (for $\Delta V_p = 900\text{V}$) which is about an order of magnitude larger than the expected shift produced by the strain-induced changes of the energy band gap ($\sim 10\text{meV}$). This effect, which we attribute to piezoelectricity, is of great importance not only for the data evaluation, but also for the theoretical model discussed below.

In Fig. 2(b) we report the strain-dependence of p/e for the X confined in one of the nine measured QDs. The dipole moment shifts almost linearly with F_p , i.e. with applied stress, with an average tuning range of $\langle \Delta p \rangle / e = (0.071 \pm 0.007)\text{nm}$ and an average slope of

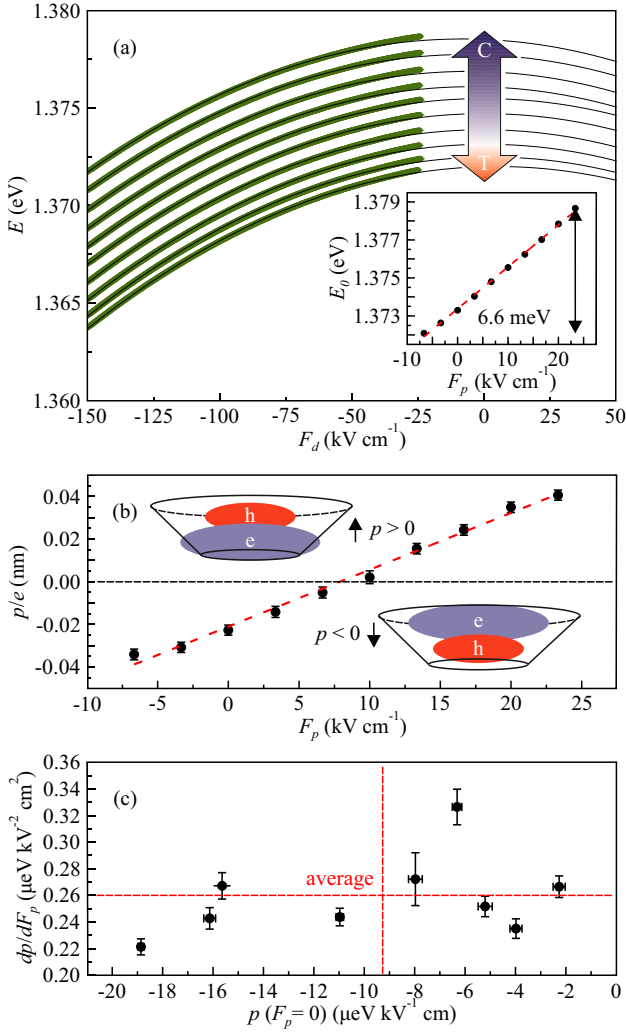


FIG. 2. (a) Determination of the stress dependence of E_0 , p and β for voltages V_p in the range from $V_p = -200$ V up to $V_p = 700$ V. The measured data (green points) are fitted with Eq. (1) (black lines) to extract E_0 , p and β . In the inset, the linear shift of E_0 with F_p is shown. The change in carrier separation p/e of X is shown in panel (b). The sketches illustrate the strain-induced inversion of the alignment of the electron and hole wave functions. The values obtained for p at $F_p = 0$ for all measured excitons are provided in panel (c) along with the corresponding tuning rates dp/dF_p .

$\langle dp/dF_p \rangle = (0.26 \pm 0.04) \mu\text{eV kV}^{-2} \text{cm}^2$. Most importantly, the applied stress is sufficient to suppress the electric dipole and invert its sign, i.e. *to swap the position of electron and hole wave functions* inside the QD. The inversion of p has been observed in four out of the nine measured QDs, and it is mainly determined by the value of p for $F_p = 0$, see Fig. 2(c). This is found to be always negative, i.e. at $F_p = 0$ the hole (electron) tends to be located closer to the QD apex (base). The measured (linear) strain-induced shift of the zero-field transition energy E_0 [$dE_0/dF_p = (0.21 \pm 0.02) \mu\text{eV kV}^{-1} \text{cm}$] is in good agreement with previous works^{2,19}. The full set

of data including E_0 , p and β for all transitions can be found in the Supplemental Material²⁴.

IV. DETERMINATION OF STRESS CONFIGURATION

To explain the physics underlying the inversion of the X built-in dipole moment, it is fundamental to gain knowledge of the type of in-plane stress delivered by the PMN-PT actuator. Any in-plane stress configuration can be described by the three independent components of the stress tensor (s_{xx} , s_{yy} and s_{xy}) or, equivalently, by two principal stresses S_1 , S_2 applied at an angle α with respect to a crystal axis ([100] in our case). The two sets of three independent parameters are related to each other via $s_{xx,yy} = \frac{S_1+S_2}{2} \pm \frac{S_1-S_2}{2} \cos(2\alpha)$ and $s_{xy} = \frac{S_1-S_2}{2} \sin(2\alpha)$. Therefore, an arbitrary in-plane stress can be fully characterized by $S_1 - S_2$, $S_1 + S_2$, and α . This requires the knowledge of several observables as F_p is varied. In our experiment we monitor (i) the shift of the X transition energy ΔE_0 [see inset of Fig. 2(a)], (ii) the changes of the magnitude of the FSS along with the corresponding X polarization angle, and (iii) the shift of the I - V trace of the diode. Point (i) is related to the hydrostatic part of the stress given by $\Delta E_0 = \tilde{a}(S_1 + S_2)$, where \tilde{a} is a parameter related to the elastic constants renormalized by the deformation potentials. Since \tilde{a} is known²⁵, we can estimate $S_1 + S_2$. Next, we use (ii) to estimate the direction α of the applied stress by using a recently developed model for the X Hamiltonian^{25,26}. For the QDs investigated in this work we estimate $\alpha = 55^\circ$ (note that $\alpha = 45^\circ$ correspond to [110] direction), as discussed in the Supplemental Material²⁴. Finally, we exploit (iii) to estimate s_{xy} and, since α is known, $S_1 - S_2$ (see later in the text). As the shift of the I - V trace onset is a quite peculiar phenomenon, we discuss its origin below.

As mentioned, the measured shift of the I - V trace cannot be accounted for by the strain-induced change of the $i\text{-Al}_{0.4}\text{Ga}_{0.6}\text{As}$ band gap. In highly doped n-type GaAs the Fermi level (E_F) lies inside the conduction band²⁷, and there is a potential difference at the interface between a semiconductor and a metal stemming from their different work functions²⁸. Although there are several possibilities of the arrangement^{28,29} we restrict ourselves (motivated by a typical scenario for n-type GaAs/Au interface³⁰) to the case when a Schottky barrier ϕ_{sb} is present at the Au contacts to the p-i-n diode³¹. Under this condition, the observed I - V shift stems from a strain-induced modification of ϕ_{sb} . More specifically, for $V_p \neq 0$ piezoelectric charges are generated at the edges of our structure as well as at every interface between two different materials. As illustrated via the band scheme in Fig. 3(a) these charges produce an additional potential θ at the Au contacts, which effectively changes the current onset in the I - V trace²². Furthermore, an additional (net) electric field F_{qd} is created in the inner

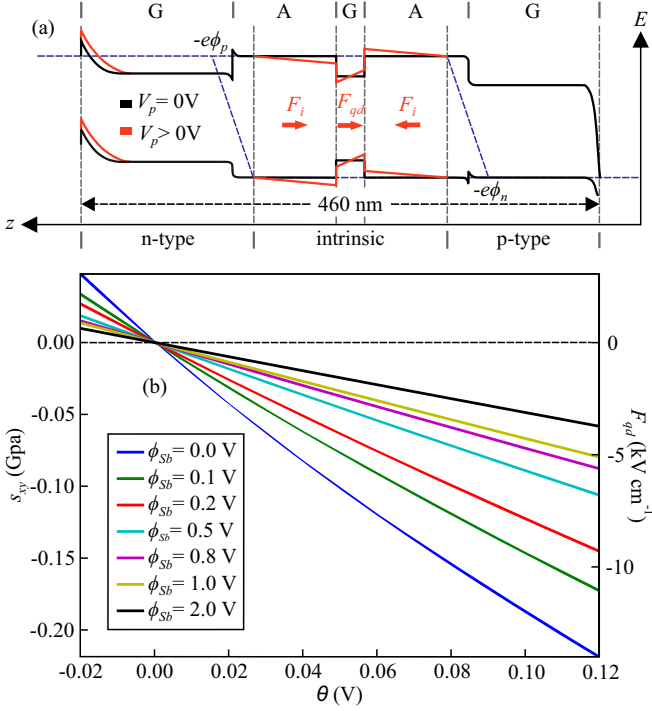


FIG. 3. (a) Schematic band profile of the studied diode. Hereby $-e\phi_n$ and $-e\phi_p$ denote the quasi-Fermi-levels for electrons and holes, respectively. G and A simply label the different materials GaAs and Al_{0.4}Ga_{0.6}As. The red curve indicates the strain-induced changes in the band alignment. In panel (b) the induced shear stress s_{xy} in the GaAs layer containing the QDs as well as the resulting electric field F_{qd} are plotted as a function of θ for several (initial) values of the Schottky barrier ϕ_{sb} .

i-GaAs layer which acts on the QDs hosted therein. The magnitude and direction of F_{qd} depends on the applied stress (T or C) as well as on the arrangement of different materials³². The surface (piezoelectric) charge density σ_p at the n-GaAs/Au interface is linked to the shear stress via $\sigma_p = e_{14}^n \tilde{S}_{44} s_{xy}$, where e_{14}^n is the piezoelectric constant of n-GaAs and \tilde{S}_{44} is one of the elastic compliance constants. By obtaining a relation between σ_p and θ we can therefore exploit the measured shift of the I - V trace onset to calculate s_{xy} (and therefore $S_1 - S_2$). The obtained dependence of s_{xy} on θ as well as of the additional electric field in the QD layer F_{qd} that is related to piezoelectric charges is shown in Fig. 3(b). The corresponding relations and their derivation are provided in the Supplemental Material²⁴. The sensitivity of s_{xy} and F_{qd} on θ is evident, especially for the small values of ϕ_{sb} typical for our structure at low temperature (we estimated 0.1 V for the doping concentration of $5 \cdot 10^{18} \text{ cm}^{-3}$ present in the n-GaAs³⁰).

The knowledge of the shear part of the stress allows us to calculate $S_1 - S_2$ for each value of F_p and, finally, magnitude, direction and anisotropy of the in-plane stress delivered by the PMN-PT. This is found to

be highly anisotropic (with a ratio $|S_1|/|S_2| \approx 3.16$), applied at 55° with respect to the $[100]$ direction and with magnitudes ($S_1 + S_2$) as high as -180 MPa (see Supplemental Material²⁴). While this stress anisotropy is not expected for the $[001]$ piezo cut used in this work, it is a common feature reported in the literature^{19,33,34}.

V. ORIGIN OF THE DIPOLE INVERSION

On this basis we performed calculations of the electronic structure of In(Ga)As QDs and investigate their dependence on the externally applied stress. The single-particle electronic levels were obtained by using the envelope function approximation based on the eight-band $\mathbf{k} \cdot \mathbf{p}$ method for electrons and holes employing the NEXTNANO³ software package³⁵. The simulated QD was assumed to be of truncated cone shape with a radius of 20 nm (10 nm) at its base (apex) and a height of 3.5 nm. The QD was embedded in a GaAs host and consisted of an In_xGa_{1-x}As alloy with the In content linearly increasing from base ($x = 0.45$) to apex ($x = 0.8$)³⁶. The externally applied stress was simulated by changing the corresponding elements of the Bir-Pikus Hamiltonian³⁷ and the calculations were performed in self-consistent Poisson-Schrödinger equation loops.

The calculations furthermore account for the effect(s) induced by piezoelectric fields. Following the common definition, the piezoelectric response of a material is given in terms of the created polarization \mathbf{P} which can be expanded as

$$P_i = \sum_{j=1}^6 e_{ij} \epsilon_j + \frac{1}{2} \sum_{jk=1}^6 B_{ijk} \epsilon_j \epsilon_k + \dots \quad (2)$$

where ϵ represents the independent components of the strain tensor in Voigt notation (i.e. $\epsilon_1 = \epsilon_{xx}$, $\epsilon_2 = \epsilon_{yy}$, $\epsilon_3 = \epsilon_{zz}$, $\epsilon_4 = 2\epsilon_{yz}$, $\epsilon_5 = 2\epsilon_{xz}$ and $\epsilon_6 = 2\epsilon_{xy}$) and e and B are the linear and nonlinear piezoelectric coefficients, respectively³⁸. In zinc-blende crystals only four independent coefficients e_{14} , B_{114} , B_{124} and B_{156} are nonzero due to symmetry considerations³⁹. The importance of the different-order contributions to the piezoelectric polarization depends essentially on the magnitude of strain and its particular configuration in the considered material and/or structure. Differently from the diode model presented above, where the relatively small applied stresses (or equivalently strains) justify the use of the linear contribution only, the strain field around and inside the QD is at least an order of magnitude larger. Therefore the nonlinear response is expected to be strongly magnified and can even dominate⁷. It is consequently reasonable to include at least the second-order contributions whereby the values for linear and quadratic piezoelectric coefficients were taken from Ref. 3 (cubic terms are expected to be negligible⁴⁰).

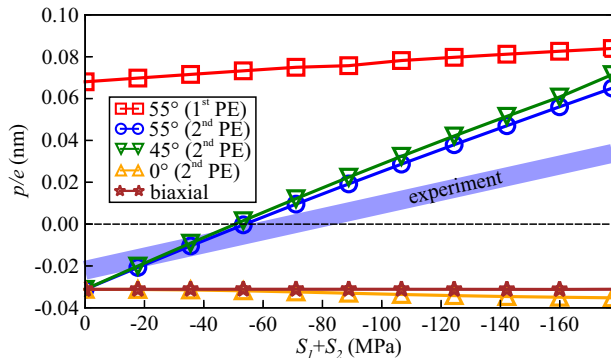


FIG. 4. The dependence of p/e on applied stress is shown for several configurations. The configuration estimated for our structure ($\alpha = 55^\circ$) is plotted with (blue) and without (red) taking into account the second-order term of the piezoelectric field. Stress fields with same anisotropy and magnitude but with S_1 aligned along $[110]$ (green, $\alpha = 45^\circ$) and $[100]$ (yellow, $\alpha = 0^\circ$) directions and for the case of purely biaxial stress (brown) are also provided.

In Fig. 4 we present the dependence of p/e on $S_1 + S_2$ for the stress configuration we estimated above with and without taking into account the second-order term of the piezoelectric field. Furthermore, we show the results obtained for stress fields with the same anisotropy and magnitude but with S_1 aligned along the $[110]$ direction (i.e., the direction which maximizes the piezoelectric effect), the $[100]$ direction (no piezoelectricity present), as well as for the case of purely biaxial stress (no piezoelectricity present).

A rich scenario can be observed. First, we notice that no appreciable variation of p/e can be observed for $s_{xy} = 0$, that is, in the absence of the piezoelectric effect (see the brown and the orange lines in Fig. 4). In strong contrast, for the stress configuration estimated above (blue line) and for a similar one in which the piezoelectric field is maximized (green line), we observe a variation of the dipole moment comparable to the experimental observations. The discrepancy between the experimental and theoretical values of p (and absolute value of E_0) is probably due to the specific QD shape considered for the theoretical calculations, which probably differs from the experimental one. It is also likely that the strain configuration we estimated is not exactly the one experienced by the specific QD due to strain inhomogeneities across the membranes. Nonetheless, our calculations clearly show that *the change in the dipole moment observed in the experiment can be only explained by the anisotropic strain configurations which switch on the piezoelectric effect*. Moreover, the large tuning rates achieved in the experiment can only be reproduced by including the second-order contribution to the piezoelectric field as apparent from the red line in Fig. 4. Thus, the inversion of the exciton dipole moment we report in this work constitutes clear and rare experimental evidence of the importance of the nonlinear terms of the piezoelectric

field in III-V QD systems.

It is worth emphasizing that, while in the calculations of Fig. 4 we used the values of the nonlinear piezoelectric coefficients reported in Ref. 3 there are several works^{4,6,38,40} that have reported different values for these coefficients. In the Supplemental Material²⁴ we discuss this point in detail and we show that the results of our calculations and our findings are preserved upon exchange of the values of the piezoelectric coefficients reported in Refs. 3, 6, 38, and 40. We would also like to mention that we approximated the (experimental) absolute value of p/e at $F_p = 0$ in the performed calculations by theoretically considering a shear pre-stress of $s_{xy}^{pre} = 200$ MPa. This pre-stress, which is already present in our device at $F_p = 0$, is a common feature and is attributed to the bonding and poling process^{33,34}. However, it has no qualitative influence on the presented behavior of p/e vs $S_1 + S_2$, which, obviously, purely depends on the applied stress (which is estimated from the experimental data).

VI. CONCLUSION

In conclusion, we have demonstrated experimentally and theoretically that piezoelectric fields can be used to engineer the wave function of excitons confined in In(Ga)As QDs and that, in this phenomenon, the nonlinear terms of the piezoelectric field dominate over the linear term. Our results are relevant not only for fundamental physics, because the effect of the piezoelectric field on the few-particle states in QDs can be now pinpointed from the experiments, but also for future applications. In fact, piezoelectricity can be used to modify the radiative lifetime, similar to vertical electric fields¹⁸. Moreover, the dipole moment can be engineered to limit the interaction of excitons with charges in the vicinity of the QD⁴¹ or to modify the response of QDs to electric fields⁴². In this context, it is worth noting that the tunability of the exciton dipole moment offered by the piezoelectric field is at least an order of magnitude larger than what can be obtained using magnetic fields⁴³ and, in addition, can be achieved using a compact and scalable approach.

ACKNOWLEDGMENTS

This work was financially supported by the European Research council (ERC) under the European Union's Horizon 2020 Research and Innovation Programme (SPQRel, Grant agreement No. 679183) and by the European Union Seventh Framework Programme 209 (FP7/2007-2013) under Grant Agreement No. 601126 210 (HANAS). P. K. and J. H. have been financially supported by the Ministry of Education, Youth and Sports of the Czech Republic under the project CEITEC 2020

(LQ1601). Furthermore, we acknowledge E. Magerl,

R. Singh, G. Bester, P. Atkinson and O. G. Schmidt for fruitful discussions and support.

-
- * johannes.aberl@jku.at
 † klenovsky@physics.muni.cz
 ‡ rinaldo.trotta@jku.at
- ¹ I. Aharonovich, D. Englund, and M. Toth, *Nature Photon.* **10**, 631 (2016).
 - ² R. Trotta, E. Zallo, E. Magerl, O. G. Schmidt, and A. Rastelli, *Phys. Rev. B* **88**, 155312 (2013).
 - ³ G. Bester, X. Wu, D. Vanderbilt, and A. Zunger, *Phys. Rev. Lett.* **96**, 187602 (2006).
 - ⁴ M. A. Migliorato, D. Powell, A. G. Cullis, T. Hammer-schmidt, and G. P. Srivastava, *Phys. Rev. B* **74**, 245332 (2006).
 - ⁵ M. A. Migliorato, J. Pal, R. Garg, G. Tse, H. Y. Al-Zahrani, U. Monteverde, S. Tomi, C.-K. Li, Y.-R. Wu, B. G. Crutchley, et al., *AIP Conference Proceedings* **1590**, 32 (2014).
 - ⁶ M. A. Caro, S. Schulz, and E. P. O'Reilly, *Phys. Rev. B* **91**, 075203 (2015).
 - ⁷ G. Bester, A. Zunger, X. Wu, and D. Vanderbilt, *Phys. Rev. B* **74**, 081305 (2006).
 - ⁸ A. Schliwa, M. Winkelnkemper, and D. Bimberg, *Phys. Rev. B* **79**, 075443 (2009).
 - ⁹ M. Winkelnkemper, A. Schliwa, and D. Bimberg, *Phys. Rev. B* **74**, 155322 (2006).
 - ¹⁰ G. Hönig, S. Rodt, G. Callsen, I. A. Ostapenko, T. Kure, A. Schliwa, C. Kindel, D. Bimberg, A. Hoffmann, S. Kako, et al., *Phys. Rev. B* **88**, 045309 (2013).
 - ¹¹ C. Segarra, J. I. Climente, A. Polovitsyn, F. Rajadell, I. Moreels, and J. Planelles, *J. Phys. Chem. Lett.* **7**, 2182 (2016).
 - ¹² M. Gong, K. Duan, C.-F. Li, R. Magri, G. A. Narvaez, and L. He, *Phys. Rev. B* **77**, 045326 (2008).
 - ¹³ M. Zieliński, *J. Phys.: Condens. Matter* **25**, 465301 (2013).
 - ¹⁴ P. W. Fry, I. E. Itskevich, D. J. Mowbray, M. S. Skolnick, J. J. Finley, J. A. Barker, E. P. O'Reilly, L. R. Wilson, I. A. Larkin, P. A. Maksym, et al., *Phys. Rev. Lett.* **84**, 733 (2000).
 - ¹⁵ M. Grundmann, O. Stier, and D. Bimberg, *Phys. Rev. B* **52**, 11969 (1995).
 - ¹⁶ A. Levin, A. Patanè, F. Schindler, A. Polimeni, L. Eaves, P. Main, and M. Henini, *Phys. Status Solidi B* **224**, 37 (2001).
 - ¹⁷ S. Germanis, C. Katsidis, S. Tsintzos, A. Stavrinidis, G. Konstantinidis, N. Florini, J. Kioseoglou, G. P. Dimitrakopoulos, T. Kehagias, Z. Hatzopoulos, et al., *Phys. Rev. Applied* **6**, 014004 (2016).
 - ¹⁸ A. J. Bennett, R. B. Patel, J. Skiba-Szymanska, C. A. Nicoll, I. Farrer, D. A. Ritchie, and A. J. Shields, *Appl. Phys. Lett.* **97**, 031104 (2010).
 - ¹⁹ R. Trotta, E. Zallo, C. Ortix, P. Atkinson, J. D. Plumhof, J. van den Brink, A. Rastelli, and O. G. Schmidt, *Phys. Rev. Lett.* **109**, 147401 (2012).
 - ²⁰ R. Trotta, P. Atkinson, J. D. Plumhof, E. Zallo, R. O. Rezaev, S. Kumar, S. Baunack, J. R. Schröter, A. Rastelli, and O. G. Schmidt, *Adv. Mater.* **24**, 2668 (2012).
 - ²¹ C. E. Kuklewicz, R. N. E. Malein, P. M. Petroff, and B. D. Gerardot, *Nano Lett.* **12**, 3761 (2012).
 - ²² Y. Zhang, Y. Liu, and Z. L. Wang, *Adv. Mater.* **23**, 3004 (2011).
 - ²³ J. J. Finley, M. Sabathil, P. Vogl, G. Abstreiter, R. Oulton, A. I. Tartakovskii, D. J. Mowbray, M. S. Skolnick, S. L. Liew, A. G. Cullis, et al., *Phys. Rev. B* **70**, 201308 (2004).
 - ²⁴ See Supplemental Material at <http://link.aps.org/supplemental/10.1103/PhysRevB.96.045414> for experimental and theoretical details.
 - ²⁵ R. Trotta, J. Martín-Sánchez, I. Daruka, C. Ortix, and A. Rastelli, *Phys. Rev. Lett.* **114**, 150502 (2015).
 - ²⁶ R. Trotta, J. Martín-Sánchez, J. S. Wildmann, G. Piredda, M. Reindl, C. Schimpf, E. Zallo, S. Stroj, J. Edlinger, and A. Rastelli, *Nat. Commun.* **7**, 10375 (2016).
 - ²⁷ J. S. Blakemore, *J. Appl. Phys.* **53**, R123 (1982).
 - ²⁸ K. K. Ng, *Complete guide to semiconductor devices* (McGraw-Hill, New York, 1995).
 - ²⁹ A. M. Cowley and S. M. Sze, *J. Appl. Phys.* **36**, 3212 (1965).
 - ³⁰ M. K. Hudait and S. B. Krupanidhi, *Physica B* **307**, 125 (2001).
 - ³¹ J. H. Werner and H. H. Güttler, *J. Appl. Phys.* **69**, 1522 (1991).
 - ³² X. Huang, C. Du, Y. Zhou, C. Jiang, X. Pu, W. Liu, W. Hu, H. Chen, and Z. L. Wang, *ACS Nano* **10**, 5145 (2016).
 - ³³ S. Kumar, E. Zallo, Y. H. Liao, P. Y. Lin, R. Trotta, P. Atkinson, J. D. Plumhof, F. Ding, B. D. Gerardot, S. J. Cheng, et al., *Phys. Rev. B* **89**, 115309 (2014).
 - ³⁴ D. Ziss, J. Martín-Sánchez, T. Lettner, A. Halilovic, G. Trevisi, R. Trotta, A. Rastelli, and J. Stangl, *J. Appl. Phys.* **121**, 135303 (2017).
 - ³⁵ S. Birner, T. Zibold, T. Andlauer, T. Kubis, M. Sabathil, A. Trellakis, and P. Vogl, *IEEE Trans. Electron Devices* **54**, 2137 (2007).
 - ³⁶ L. Wang, A. Rastelli, S. Kiravittaya, R. Songmuang, O. Schmidt, B. Krause, and T. Metzger, *Nanoscale Res. Lett.* **1**, 74 (2006).
 - ³⁷ G. L. Bir, G. E. Pikus, *Symmetry and Strain-Induced Effects in Semiconductors* (Wiley, New York, 1974).
 - ³⁸ A. Beya-Wakata, P.-Y. Prodhomme, and G. Bester, *Phys. Rev. B* **84**, 195207 (2011).
 - ³⁹ H. Grimmer, *Acta Crystallogr. Sect. A* **63**, 441 (2007).
 - ⁴⁰ G. Tse, J. Pal, U. Monteverde, R. Garg, V. Haxha, M. Migliorato, and S. Tomić, *J. Appl. Phys.* **114**, 073515 (2013).
 - ⁴¹ G. Callsen and G. M. O. Pahn, *Phys. Status Solidi (RRL)* **9**, 521 (2015).
 - ⁴² C. L. Salter, R. M. Stevenson, I. Farrer, C. A. Nicoll, D. A. Ritchie, and A. J. Shields, *Nature* **465**, 594 (2010).
 - ⁴³ S. Cao, J. Tang, Y. Gao, Y. Sun, K. Qiu, Y. Zhao, M. He, J.-A. Shi, L. Gu, D. A. Williams, et al., *Sci. Rep.* **5**, 8041 (2015).